Journal of Cleaner Production 371 (2022) 133647

Contents lists available at ScienceDirect

Journal of Cleaner Production

journal homepage: www.elsevier.com/locate/jclepro

A clean dispersant for nano-silica to enhance the performance of cement mortars

Xin Qian [a,b], Jialai Wang [b,*], Liang Wang [b,c], Yi Fang [b,**], Peiyuan Chen [c], Mengxiao Li [a]

[a] Key Laboratory of Infrastructure Durability and Operation Safety in Airfield of CAAC, Tongji University, Shanghai, 201804, PR China
[b] Department of Civil, Construction, and Environmental Engineering, The University of Alabama, Tuscaloosa, AL, 35487, USA
[c] School of Civil Engineering and Architecture, Anhui University of Science and Technology, Huainan, Anhui, 232001, PR China

ARTICLE INFO

Handling Editor: Zhen Leng

Keywords:
Nano-silica
Tannic acid
Dispersant
Microstructure
Compressive strength

ABSTRACT

Nanoparticles can be used to enhance the performance of concretes. However, dispersants (surfactants) are commonly needed to overcome the aggregation/agglomeration of nanoparticles. Existing dispersants are mainly petroleum-based products. Their manufacturing and incorporation into concretes can have a harmful impact on the environment. To address this issue, this study proposes using an edible, plant-based product, tannic acid (TA), as a clean dispersant for colloidal nano-silica (CNS) in concretes. This can be done by simply mixing CNS particles with a TA solution. The produced CNS suspension can then be used as the mixing water to make cement mortars. Experimental studies suggest that a layer of TA is coated onto the silica nanoparticle, producing a TA-SiO_2 biohybrid nanoparticle. Particle distribution analysis shows that this TA layer on the CNS is around 4.35 nm. The TA coating not only prevents the aggregation/agglomeration of nanoparticles but also delays the pozzolanic reaction between the nano-silica and calcium hydroxide (CH) in the concrete, making them available for filling nanopores in the hydrated cement paste. As a result, the microstructure of the produced cement paste is densified, as confirmed by mercury intrusion porosimetry, scanning electron microscopy, and nanoindentation testing. Particularly, capillary pores smaller than 50 nm are significantly reduced by the new biohybrid nanoparticles. This leads to 37% improvement in the compressive strength at 28d of the cement mortar with the TA dispersed CNS over that of the mortar made without using TA to disperse CNS.

1. Introduction

Extensive studies have shown that the performance of Ordinary Portland cement (OPC)-based concrete can be significantly improved by adding nanoparticles through a few mechanisms: a) providing nucleation seeding sites for hydration products to promote the hydration of OPC, b) filling the pores in the concrete to produce dense microstructure, c) reacting with hydration products to produce more binding materials, and 4) reinforcing hardened cement paste. Nano-silica (SiO_2) is one of the most commonly used nanoparticles in concrete (Abhilash et al., 2021) because of its exceptional pozzolanic reactivity compared to other nanoparticles. Calcium silicate hydrate (C–S–H) gel can be produced through the rapid reaction between calcium ions released from OPC and nano-silica, and they, as well as nano-silica itself, can serve as "seeds" for the hydration of cement. Many benefits can be achieved by adding nano-silica into concrete, including higher mechanical properties, faster hydration rate, and better durability (Abhilash et al., 2021). For example, Mukharjee and Barai (2020) reported that the compressive strength of cement mortar could be enhanced by 20% at 28d with 3% nano-silica replacement.

However, real applications of nanoparticles in concrete are very limited because of the low benefit-cost ratio induced by the high cost and difficulty of dispersion of nanoparticles. Similar to other nanoparticles, nano-silica cannot be easily dispersed because of high Van Der Waals interactions induced by its high specific surface area. Existing studies show that the aggregation/agglomeration of nano-silica is inevitable in dry powder. Colloidal nano-silica (CNS) (silica sol) may provide better dispersion than dry powder (Kong et al., 2019). It still gels or coagulates immediately after being mixed with cement and water (Kong et al., 2013) due to the rapid increase of ionic strength in the cement paste/concrete, leading to a significant reduction of workability. As a result, the effectiveness of using nano-silica to improve the

* Corresponding author.
** Corresponding author.
E-mail addresses: jwang@eng.ua.edu (J. Wang), yfang20@crimson.ua.edu (Y. Fang).

https://doi.org/10.1016/j.jclepro.2022.133647
Received 23 February 2022; Received in revised form 28 July 2022; Accepted 13 August 2022
Available online 21 August 2022

performance of concrete is significantly reduced.

A few methods have been proposed to address these drawbacks. For example, a dispersant such as polycarboxylate (PCE) is commonly used to disperse the nano-silica in fresh concrete and compensate for the loss of workability induced by the nano-silica (Chithra et al., 2016; Korayem et al., 2017). However, Fernández et al. found little interaction between common commercialized PCE and nano-silica in the lime mortar (Fernández et al., 2013), indicating nano-silica cannot be thoroughly dispersed by simply mixing PCE and nano-silica. In order to solve this problem, efforts have been made to modify the surface of nanoparticles (Collodetti et al., 2014; Gao et al., 2017; Gu et al., 2016; Li et al., 2018; Lu et al., 2017). Collodetti et al. (2014) grafted siloxanes on nano-silica particles to delay the pozzolanic reaction of nano-silica so that more nano-silica particles could be available to fill the capillary pores of the concrete. Gu et al. functionalized CNS with silanized polycarboxylate superplasticizer by a "grafting to" method. Their method produced nanoSiO_2@PCE core-shell nanoparticles, which are more stable in the saturated CH solution, resulting in promoted hydration of cement (Gu et al., 2016). Nevertheless, these existing functionalization methods are far from perfect. For example, siloxane functionalization can significantly retard the hydration of cement (Collodetti et al., 2014), while using nanoSiO_2@PCE core-shell nanoparticles can substantially increase the cost of the nanoparticles.

Petroleum-based chemicals are predominately used in these studies. Manufacturing these chemicals can consume a large amount of energy and generate high carbon emissions, as well as by-product sludge. Since these chemicals are readily soluble in water, they can leach out of concretes, posing a potential environmental threat. Thus, low-cost, clean, and environmentally friendly dispersants are needed, which can be used to replace existing chemicals to promote the dispersion of the nanoparticles in concretes. To this end, this study explores a naturally occurring chemical compound, tannic acid (TA), as an eco-friendly dispersant for nano-silica. TA is a water-solvable plant polyphenol and is the world's third largest class of plant components after cellulose and lignin (Hagerman et al., 1998). It can be written as $C_{76}H_{52}O_{46}$ with a chemical structure shown in Fig. 1(b). It has a center glucose molecule and five hydroxyl moieties esterified with two gallic acid (3,4,5-trihydroxybenzoic acid) molecules. With abundant reactive terminal phenolic hydroxyl groups, TA has the ability to complex or cross-link macromolecules at multi-binding sites through multiple interactions, including hydrogen and ionic bonding and hydrophobic interactions (Chen et al., 2022). TA can be extracted from plants, microorganisms (Fei et al., 2017), or decomposing organic matters in water (Liu et al., 2015).

Dispersion of nano-silica can be carried out by mixing CNS with a TA solution, as shown in Fig. 1. The use of TA not only prevents the aggregation/agglomeration of nanoparticles but also delays the pozzolanic reaction between nano-silica and CH in the concrete, making these nanoparticles available to fill nanopores in the material. As a result, the workability and compressive strength of the concrete can be improved by adding these biohybrid nanoparticles, as revealed by this study. Compared with existing petroleum-based agents used to disperse nano-silica, naturally occurring product TA enjoys many advantages such as abundant, renewable, safe, non-toxic, and cost-effective (Schieber et al., 2001).

In addition to dispersing the nano-silica, two extra benefits are provided by TA. First, TA can interfere with the hydration of the cement to in-situ produce more nanoparticles in the fresh concrete, which can be used to further densify the microstructure of the produced concrete (Fang et al., 2021). Second, TA can function as a cathodic-type corrosion inhibitor, retarding the cathodic process of the corrosion reactions by forming ferric tannates on the mild steel surface (Kusmierek and Chrzescijanska, 2015). This is because TA can easily react with the initial rust c-FeOOH to form the TA-iron complex, which will be oxidized to ferric tannate. Ferric tannate is stable and much denser than steel rust, acting as a physical barrier to protect the reinforcing steel in concrete from corrosion.

2. Materials and methods

2.1. Materials

Type I/II OPC with a median diameter (D50) of 15.37 μm was used to prepare cement paste and mortar samples. Its oxide composition obtained from X-ray fluorescence (XRF) is presented in Table 1. The fine aggregates used in this study were river sand with a bulk specific gravity of 2.70 and a water absorption capacity of 0.95%. These river sand were oven-dried for 12 h at 100 °C before being mixed with other ingredients. The TA used in this study has a purity of 98%. The CNS has an average particle size of 20 nm and contains 50 wt% solid content.

2.2. Characterization of TA dispersed CNS suspension

2.2.1. Particle size distribution

The sizes of particles in CNS suspensions with and without TA were measured by dynamic light scattering (DLS, Zetasizer Nano ZS DLS system, Malvern Instruments Ltd.). The TA was first dissolved in the deionized water to produce a TA solution. Then CNS suspension was

Table 1
Chemical composition of Type I/II Portland cement.

Oxide Composition	Type I/II Portland cement (%)
SiO_2	21.78
Al_2O_3	6.1
Fe_2O_3	3.24
MgO	0.83
CaO	66.9
Na_2O	0.1
K_2O	0.57
LOI	2.58

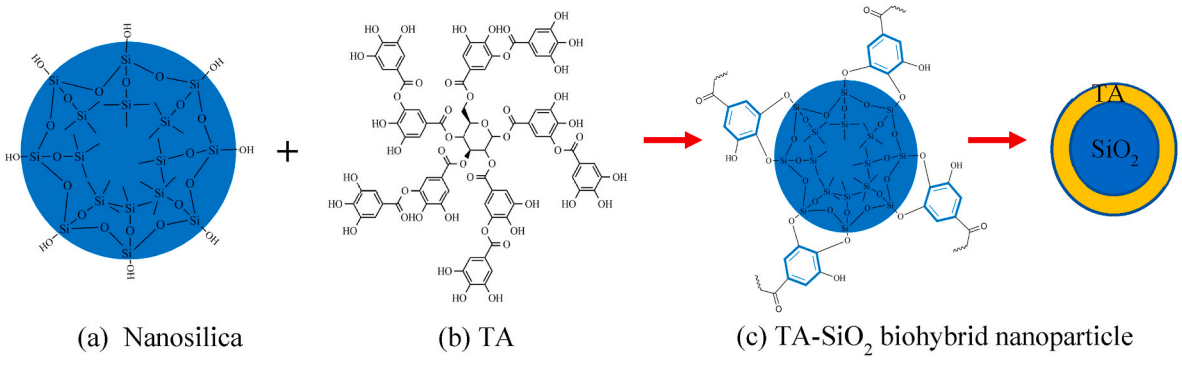

Fig. 1. Functionalizing CNS using TA to produce TA-SiO_2 biohybrid nanoparticles.

added into the TA solution under stirring to disperse CNS particles.

2.2.2. Fourier-transform infrared spectrometer (FTIR)

A Perkinelmer Paragon 1000 FTIR was used to examine potential interaction between CNS particles and the TA. The spectral range used in this analysis is 4000-650 cm^{-1}, in which all the typical features of both TA and CNS can be observed. The CNS suspensions with and without TA were oven-dried at 80 °C for 24 h before the measurement.

2.2.3. Transmission electron microscope (TEM)

The morphologies of CNS nanoparticles in these suspensions were examined using the FEI Tecnai F-20 TEM with an accelerating voltage of 200 kV, as shown in Fig. 2(b). The TEM samples were prepared by depositing one drop of the suspension onto copper grids and being vacuum dried.

2.2.4. Pozzolanic reactivity

The effect of the TA coating on the pozzolanic reactivity of the CNS was examined by analyzing the reaction products between the CNS and calcium hydroxide (CH) by thermogravimetric analysis (TGA). To this end, 20 g portlandite was added into a CNS slurry which was made by dispersing 10 g CNS into a TA solution. The produced slurry was sealed and stored at room temperature of 23 °C for 24 h, 96 h, and 360 h. The reaction products were collected by vacuum filtration and washed with acetone to prevent further reaction, followed by drying in an oven at 60 °C for at least 12 h. The TGA was carried out by a Simultaneous Thermal Analyzer 8000 from PerkinElmer at a heating rate of 10 °C/min from 30 °C to 800 °C.

2.3. Characterizing the mortar specimens

2.3.1. Setting time and flowability

Vicat needle test was performed to examine the effect of TA dispersion on the set times of the produced cement pastes based on ASTM C191 (ASTM, 2021a,b). Four groups of paste samples with water to cement ratio of 0.5 were prepared: the control group without any additive, the CNS group in which 3% of OPC was replaced by the same amount of CNS, the CNS+TA group in which 3% OPC was replaced by the same amount of CNS dispersed by 0.2% TA, and the TA group in which 0.2% of TA was added. All the percentages used in this study, if not specified, are given by the weight of the cement.

Four groups of cement mortar samples were prepared for workability testing: the control group, the CNS group, the TA group, and the superplasticizer (SP) group. The Control group were made with a water to cement ratio of 0.5 and a sand to cement ratio of 2.52. The CNS group were prepared with the same mix as the control one, except that a small percentage of the cement was replaced by the same amount of the CNS. The produced mortars are noted as XC, which refers to the mortar sample with X% of the cement replaced by the CNS. The dispersed CNS mortar groups are made by replacing a small amount of cement with the same amount of CNS dispersed by 0.2%, 0.4%, and 0.6% TA. The produced mortar samples are noted as XCYT, which refers to the sample with X% of cement replaced by the same amount of the CNS functionalized with Y% of the TA. The TA group was made with the same mix as the control one, except that a small amount of the TA was added as an extra additive to the mortar. Three different concentrations of TA, 0.2%, 0.4%, and 0.6%, were used in this group, and the produced mortar samples are noted as XT, which refers to the mortar sample with X% TA added. The SP group was made as a benchmark in which the petroleum-based dispersant, polycarboxylate was used to replace TA to produce the sample. The detailed mix design of all these mortar samples is present in Table 2. The workability of these produced cement mortars was determined by the flow table test according to ASTM C1437 (ASTM, 2015).

2.3.2. Isothermal calorimetry test

Isothermal calorimetry testing was carried out to examine the effect of TA dispersed CNS on the hydration of the cement paste based on ASTM C1679 and ASTM C1702 (ASTM, 2017, 2014). In this test, cement pastes of four mortar samples (control, TA, CNS, CNS+TA) prepared for the set time test were used. The CNS+SP paste was also made by replacing 3% of cement with CNS dispersed by 2% (by weight of cement) superplasticizer, polycarboxylate. The rate of heat release and total heat released by the hydration of the cement pastes can be directly measured using I-Cal 2000HPC and I-Cal 4000HPC from Calmetrix Incorporation.

2.3.3. Hydration products

The cement paste specimens used in this testing were prepared using the same mix as those used in calorimetry testing. After 2d and 28d of curing, all these specimens were pulverized in a sealed bag to avoid contamination and carbonation. The produced cement pastes powders with size smaller than 0.15 mm were sieved out and then examined by X-

Table 2
Mix design for cement mortars produced with/without using CNS (kg/m^3).

Groups	Cement	Water	River Sand	CNS	TA	SP
Control	360.2	180.1	907.7	–	–	–
1C	356.6	180.1	907.7	3.6	–	–
0.2T	360.2	180.1	907.7	–	0.72	–
1C0.2T	356.6	180.1	907.7	3.6	0.72	–
3C	349.4	180.1	907.7	10.8	–	–
0.4T	360.2	180.1	907.7	–	1.44	–
0.6T	360.2	180.1	907.7	–	2.16	–
3C0.2T	349.4	180.1	907.7	10.8	0.72	–
3C0.2SP	349.4	180.1	907.7	10.8	–	0.72
3C0.4T	349.4	180.1	907.7	10.8	1.44	–
3C0.6T	349.4	180.1	907.7	10.8	2.16	–
5C	342.2	180.1	907.7	18.0	–	–
5C0.2T	342.2	180.1	907.7	18.0	0.72	–

XC: mortar sample with X% cement replaced by the same amount of CNS.
XCYT: mortar sample with X% cement replaced by the same amount of CNS functionalized with Y% TA.
XT: mortar sample with X% TA added.
SP: superplasticizer (polycarboxylate).

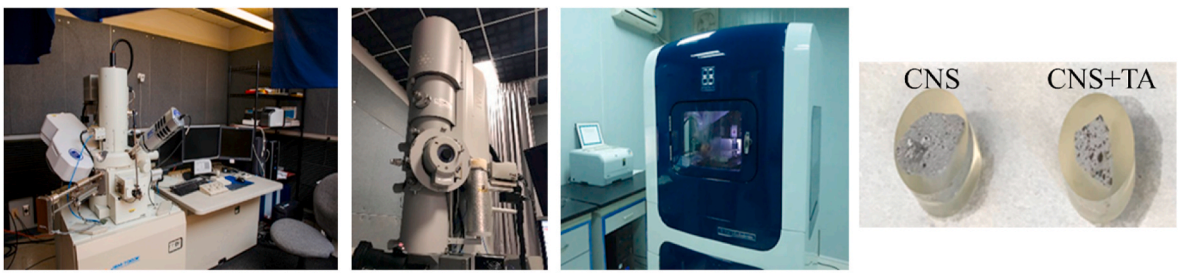

Fig. 2. Images of some testing equipment and specimens in this study: (a) JEOL 7000 FE SEM; (b) FEI Tecnai F-20 TEM; (c) Hysitron TI 950 Nanoindenter; (d) Specimens prepared for nanoindentation testing.

Ray Diffraction (XRD) and TGA to evaluate the effect of the proposed method on the hydration products of the cement. The XRD patterns were obtained by scanning between 10° - 70° with a Bruker D8 Discover at a scanning rate of 10°2θ per minute using Cu Kα radiation at 35 kV and 20 mA. For TGA, the sample was first held at 30 °C for 30 min and then heated from 30 °C to 1000 °C at 10 °C/min.

2.3.4. Microstructure

A JEOL 7000 FE Scanning Electron Microscopy (SEM), as shown in Fig. 2(a), was used to examine the microstructure of the cement paste samples, which were produced using the same mix as those used in the calorimetry test. All specimens were coated with a layer of gold (Au) to prevent charging. Their porosity and pore size distribution were further analyzed by using mercury intrusion porosimetry (MIP).

2.3.5. Grid of nanoindentation

The cement pastes were prepared with a water to cement ratio of 0.5 and cured in a sealed plastic bag for 28 d. The pastes were first cut to fit a 32.5 mm diameter capsule filled with epoxy resin. Once the epoxy resin hardened, the specimens were taken out and polished with 240, 600, 800, and 1200 grit silicon carbide sandpaper, followed by 3 μm diamond suspension, 1 μm diamond suspension, 0.3 μm alumina suspension, and 0.05 μm alumina suspension on a felt pad, as shown in Fig. 2(d). A grid of 20 × 20 nanoindentations was performed with 10 μm spacing between the measurement points on the prepared specimens by Hysitron TI950 Nanoindenter. During the indentation process, the load was increased linearly to 1 mN with multiple partial unloading, held constant for 2s, and finally decreased linearly back to zero in 5s. The Poisson ratio of the prepared cement paste specimens was assumed to be 0.2. The indentation stiffness was determined based on the unloading data between 50% and 95% of the maximum load. The indentation elastic modulus was derived using the Oliver and Pharr method for each indent (Oliver and Pharr, 1992). The packing density of the hydration products could be obtained based on a simplified linear relation (Eq. (1)), given by Refs. (Vandamme, 2008; Vandamme and Ulm, 2013):

$$M_i = m_s(2\eta_i - 1) \tag{1}$$

where η_i is the packing density (η_i = 1-porosity) at the location of the indent, M_i is the indentation modulus, and m_s is the indentation modulus of the solid phase, which is 62.5 GPa according to the reported value for solid C–S–H (Pellenq et al., 2009). The M_i is related to the Young's (E) modulus and Poisson ratio (ν) of the indented half-space:

$$M = E/(1-\nu^2) \tag{2}$$

It is essential to apply the deconvolution method to the heterogeneous and multiphase materials for determining the volume fractions and the average mechanical properties. The statistical deconvolution was processed in MATLAB by using Gauss Mixture Model (GMM) to fit the marginal probability density functions (PDF) of elastic modulus and packing density. Only the indents with elastic modulus less than 60 GPa (excluding anhydrous clinker minerals) were recognized as C–S–H phases in this paper (Pellenq et al., 2009). Four major phases of hydration products can be identified based on the deconvolution results, which are porous phases (PP, ~12 GPa), low-density C–S–H (LD, ~22.0 GPa), high-density C–S–H (HD, ~32 GPa), and composite of ultra-high density C–S–H and CH (UHD/CH, ~48.6 GPa) (Pedrosa et al., 2020).

2.3.6. Compressive strength

Four groups of mortar samples consisting of thirteen different mixes were prepared for compressive testing, as shown in Table 2. These mortar samples were cast into 50 × 100 mm cylinders, and their compressive strength were measured at ages of 3, 7, and 28d, respectively, based on ASTM C39 (ASTM, 2021a,b).

3. Results and discussion

3.1. Particles size and morphology of the produced biohybrid nanoparticles

Fig. 3(a) compares the particle size distribution of CNS suspension with and without TA. Without TA as a dispersant, the CNS suspension has a particle size distribution ranging from 6 nm to 310 nm, and most CNS particles are smaller than 50 nm. A larger size of particles up to 300 nm can also be observed in this suspension, clearly induced by the aggregation/agglomeration of the silica nanoparticles. This can be confirmed by the TEM image shown in Fig. 3(c), which clearly shows that nanoparticles are aggregated into large colloids. After dispersed by TA, a clear shift to a larger size is observed for the produced nanoparticles, as shown in Fig. 3(a). This figure shows that the peak size of the TA dispersed nanoparticle is 9.7 nm larger than that of the pristine one. This suggests that a layer of TA coating with a thickness of around 4.35 nm is formed on the surface of the silica nanoparticle to form a TA-SiO2 biohybrid nanoparticle due to covalent and non-covalent interactions induced by abundant terminal phenolic hydroxyl groups of TA (Chen et al., 2022). Fig. 3(a) also clearly shows that most particles larger than 100 nm existing in the pristine CNS suspension disappear in the TA dispersed CNS, suggesting that much better dispersion of the nanoparticles is achieved by the TA. This is also confirmed by the TEM image of the CNS particles shown in Fig. 3(d), which shows that agglomeration of CNS particles shown in Fig. 3(c) in the virgin CNS suspension is eliminated by the TA. Almost all the nanoparticles are separated from each other in this suspension.

The abundant hydroxyl groups in TA can interact with the surface of CNS, which has a large number of Si–OH groups (Zhuravlev, 2000) to form a stable seven-members ring through covalent bonds, as shown in Fig. 1. As a result, a slight reduction in wavelengths of groups, such as C=C, C=O, and C-Carom, can be observed in the FTIR spectrum of TA, as shown in Fig. 3(b). This figure compares the FTIR spectra of CNS before and after TA dispersion. The peaks at 1052 and 795 cm^{-1} correspond to symmetric and asymmetric stretching vibration peaks of Si–O, respectively. The vibration modes observed in pure TA at 1019, 1310, 1444, 1607, and 1697 cm^{-1} are C–O asymmetric stretching, aromatic CH deformation, C-Carom stretching, C=C stretching, and C=O stretching, respectively. It can be seen that the last four bands were shifted to 1346, 1454, 1617, and 1699 cm^{-1}, respectively, confirming the presence of strong interaction between the TA and silica nanoparticles.

Fig. 4 compares the TGA results of the reaction product between CNS and CH without and with TA as the dispersant. As marked in the figures, the typical decomposition temperature ranges for CH and calcium carbonate are 400°C–500 °C and 680°C–760 °C, respectively (Park et al., 2016). The weight loss starting at 105 °C and mainly occurring at 120 °C–160 °C can be attributed to the decomposition of C–S–H gel (Park et al., 2016), which is the main reaction product between the CNS and CH. It can be seen that less C–S–H gel and more CH were present in all the specimens prepared with TA dispersed CNS, suggesting that the TA coating slowed down the pozzolanic reactivity of the CNS with CH within the observed period. As a result, more silica nanoparticles are available to fill the nanopores during the hydration of cement. In addition, TA can form complex with calcium (Shnawa et al., 2015), such as calcium tannate, which can be confirmed by the right shift of the peak corresponding to the mass loss of calcite and portlandite in Fig. 4(b) and (c). The enhanced thermal stability of the portlandite and calcite is induced by the TA-calcium complex. It should be mentioned that the carbonation of calcium tannate can also produce calcite at high temperatures, thereby increasing the mass loss of calcite.

All these findings suggest that TA can be successfully coated on the surface of silica nanoparticles to produce a biohybrid nanoparticle consisting of a silica core and a nanocoating of TA due to the strong interaction between TA and the silica nanoparticle. Since TA is negatively charged, aggregation/agglomeration of the nanoparticle is

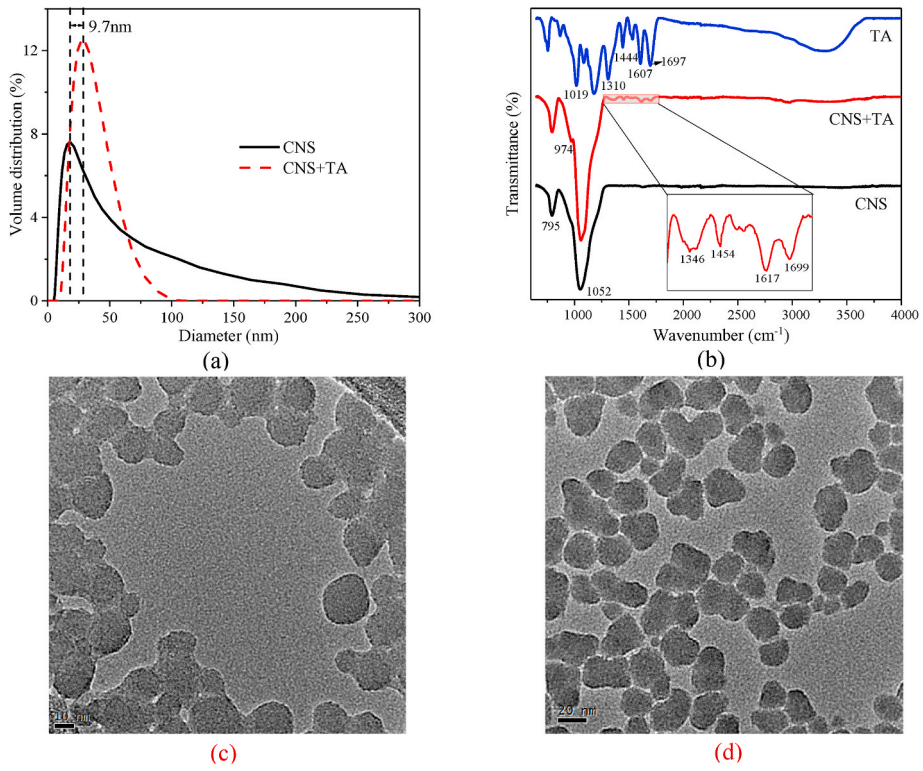

Fig. 3. Measurements of CNS with and without TA coating: (a) Particle size distribution; (b) FTIR spectra; (c) TEM image of CNS; (d) TEM image of functionalized CNS.

minimized, and homogeneous dispersion of the nanoparticle is therefore produced, as shown in Fig. 3(d). More importantly, TA coating will delay the pozzolanic reaction of the silica nanoparticles, making them available to fill the nanopores of the produced mortar/concrete.

3.2. Setting time and workability

The Vicat needle testing was employed to evaluate the effect of TA on the set time of the produced cement paste, as shown in Table 3. After replacing a small portion of cement with the CNS, both initial and final set times of the sample were significantly reduced compared with that of the control one due to the seeding effect of the nanoparticles, which can accelerate the hydration of the cement. While adding TA to the paste made these two set times much longer because TA retards the hydration of cement (Abrams, 1920). Set time closest to that of the control one was obtained using TA dispersed CNS, as shown in Table 3. In this case, the set times are longer than using the pristine CNS because the TA coating on the surface of the biohybrid nanoparticle delays the seeding effect of the nano-silica and the pozzolanic reaction between the CNS and CH. In addition, the residual TA in the suspension can also retard the hydration of the cement.

Set time testing results shown in Table 3 indicate that the hydration rate of cement can be controlled by combining nano-silica and TA. The former accelerates the hydration, while the latter retards the hydration of cement. By varying the contents of these two additives, we can adjust the set times of the cement to a range ideal for the application.

Fig. 5 compares the flowabilities of the produced mortars without and with TA. Among all mortar samples tested, the one with CNS (3C) has the lowest flowability. This confirms that CNS can significantly reduce the workability of the cement mortar, one of the major drawbacks of using nano-silica in concretes. On the contrary, the workability of the cement mortar can be improved by adding TA. It can be seen that the mortar sample achieves higher flowability with more TA used to disperse the nanoparticles. Clearly, TA can disperse cement particles too, leading to better workability. For this reason, the reduction in workability of the mortar induced by the CNS can be alleviated by dispersing the CNS with TA, as shown in Fig. 5.

3.3. Hydration heat

The effect of TA dispersion on the hydration of the cement was examined by isothermal calorimetry, and the results are shown in Fig. 6. As expected, the addition of CNS significantly accelerates the hydration of cement paste due to the seeding effect of the nanoparticles. On the contrary, the addition of TA significantly retards the hydration of the cement, and the peak corresponding to C_3S hydration is delayed to almost 24 h. This retarding effect of TA has been discovered for over one century (Abrams, 1920). Our ongoing research shows that the retarding mechanism of TA is quite unique. TA has a strong ability to capture calcium ions (Ju et al., 2017) dissolved from the cement particle to form calcium tannate nanoparticles. This process consumes most calcium ions dissolved from the cement, leading to insufficient calcium ions in the fresh concrete to produce precipitate at an early age. As a result, the dormant period of the hydration is much longer, as shown in Fig. 6. This retarding effect of TA can be offset by the accelerating effect of the nano-silica, as revealed by the calorimetry curve of the cement paste added with TA dispersed CNS. It shows that the duration of the dormant period of the mortar was shortened to almost the same as that of the control sample. In addition to the seeding effect of the nanoparticles, most TA is coated on the surface of nano-silica to form biohybrid nanoparticles, and therefore, much less TA is available to retard the hydration of the cement. As a result, two peaks corresponding to the hydration of C_3S and C_3A in the testing curve are higher than the control one. Fig. 6(b) compares the total heat released from the hydration of these cement pastes. Within the observation period, the paste with the pristine CNS generates the highest heat due to the seeding effect of the CNS, while the one with TA generates the lowest heat due to the strong retarding effect of TA. By dispersing the CNS with TA, the accumulated

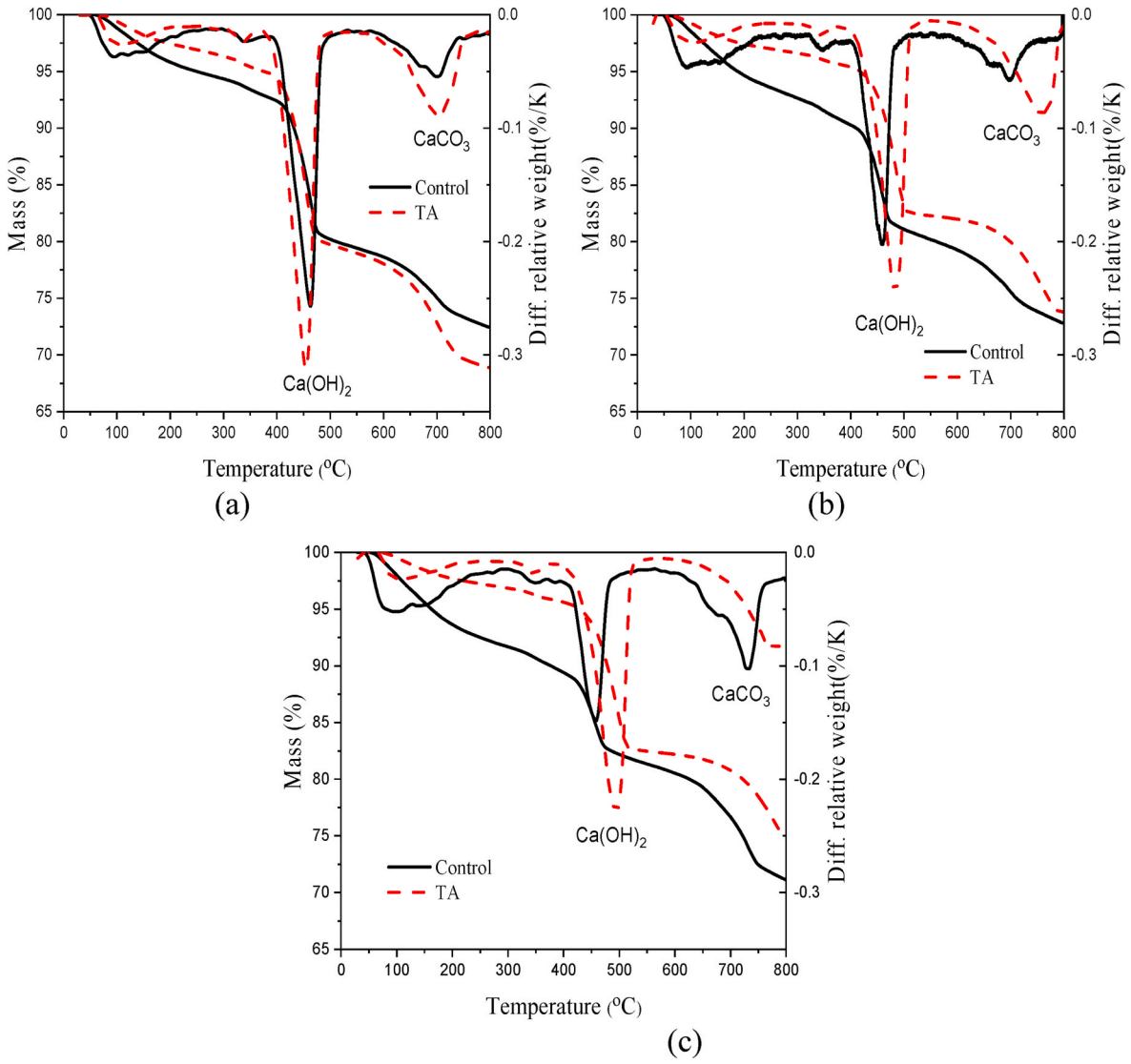

Fig. 4. Weight losses of different minerals at: (a) 24 h; (b) 96 h; (c) 360 h.

Table 3
Set times of cement pastes with and without functionalized CNS.

Group	Initial Set (min)	Final Set (min)
Control	160	257
TA	368	477
CNS	109	203
CNS+TA	148	245

energy generated by the hydration of the cement is just slightly lower than that of the group with only pristine CNS but higher than that of the control group.

The effect of dispersing the CNS with a PCE-based superplasticizer was also examined for comparison. Fig. 6(a) shows that this dispersion can slightly increase the dormant period of the cement compared to that one with pure CNS. Even though the early hydration of the cement was greatly promoted by the PCE dispersed CNS, a similar accumulated heat was observed in the hydration of the paste prepared with PCE dispersion compared to the one with TA dispersion at the end of 48 h.

3.4. Hydration products

XRD analyses were carried out to study the hydration products of

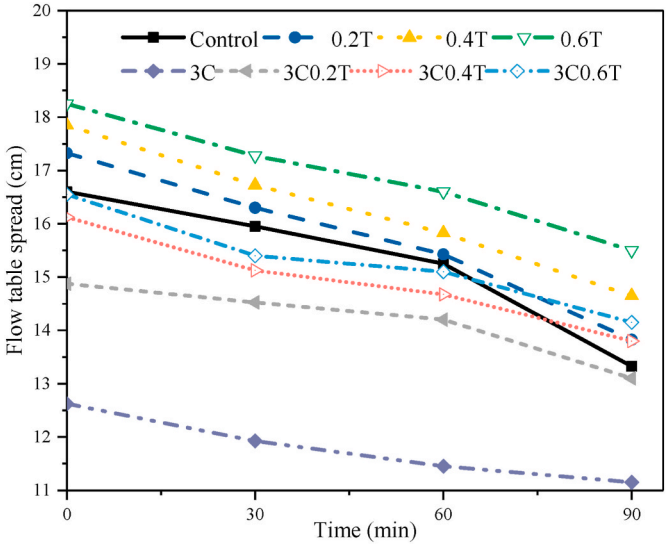

Fig. 5. Flow spread diameter of cement mortars after flow table tests.

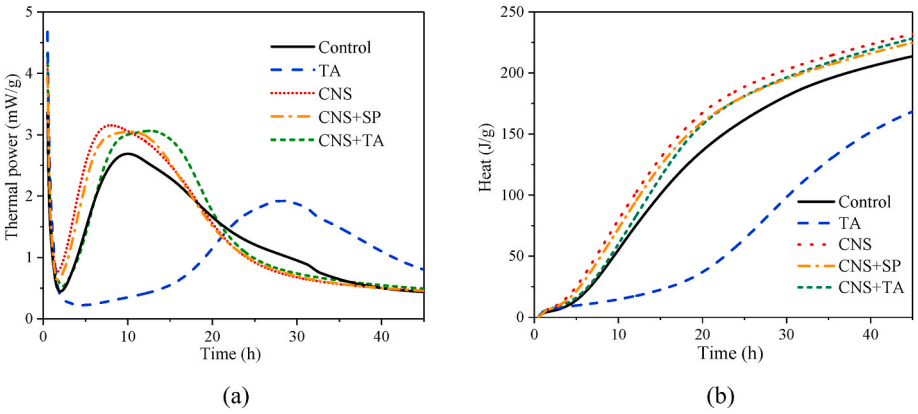

Fig. 6. Isothermal calorimetry curves of OPC pastes produced with different methods: (a) Thermal power for OPC paste for 45 h; (b) Accumulated released hydration heat of OPC paste for 45 h.

cement pastes prepared with and without TA dispersion, and the results are shown in Fig. 7. Fig. 7(a) presents the XRD spectra of the paste samples at 2d. In addition to residual C_2S and C_3S, typical hydration products such as CH, C–S–H, and ettringite can be identified from these spectra. No new mineral has been produced due to the introduction of TA as a dispersion agent. Nevertheless, the retarding effect of TA can be clearly observed from these spectra, as evidenced by the fact that the intensity of CH of the sample with TA is the weakest among all tested samples. After hydration of 28d, XRD spectra of all paste samples appear very similar, as shown in Fig. 7(b), suggesting that the retarding effect of TA diminishes at 28d.

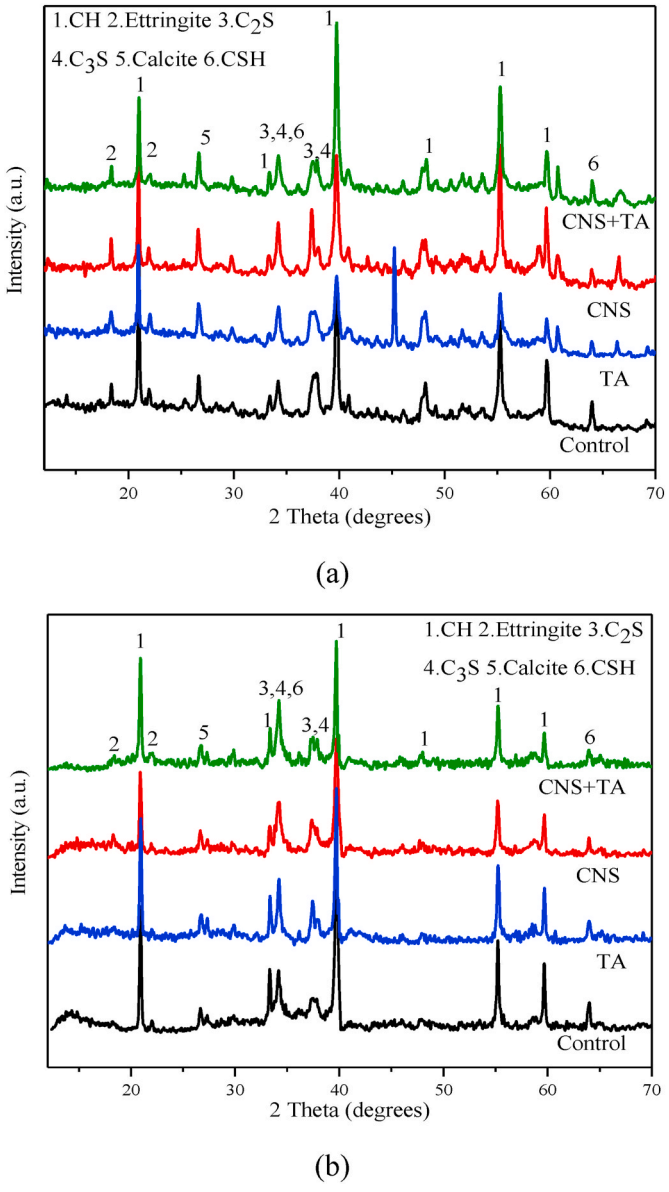

Fig. 7. XRD patterns of cement paste produced with and without functionalized CNS at: (a) 2d; (b) 28d.

Quantitative analysis of the hydration products was carried out based on TGA results, as shown in Figs. 8 and 9. The temperature ranges used to calculate weight loss due to decomposition of ettringite, AFm, CH, and calcite are 80°C–105 °C, 180°C–200 °C, 400°C–500 °C, and 680°C–760 °C, respectively (Bakolas et al., 2006; Borges et al., 2010; Hashem et al., 2013; Park et al., 2016). At 2d, the CH content in the control sample is the highest, which is expected. Some CH in the CNS sample should be consumed by the pozzolanic reaction between the CH and the nanoslica. The lower content of CH in the TA sample can be contributed to the retarding effect of TA as revealed by the calorimetry test shown in Fig. 6, which slows down the production of CH at early age. The reduction of CH content in CNS+TA sample is induced by both the retarding effect of TA and the pozzolanic reaction between the CH and nanosilica. At the same degree of hydration, the CH content in the CNS+TA sample should be lower than that in the TA sample since no pozzolanic reaction occurs in the TA group. Fig. 9(a) shows an opposite trend, indicating that the presence of the CNS facilitates the hydration of the cement. This also agrees well with the isothermal calorimetry results shown in Fig. 6.

At 2d, presence of TA appears to promote the formation of ettringite, as revealed by Fig. 9(a). This figure shows that the content of ettringite in two samples with TA are slightly higher than the control group. Similar phenomenon was observed in the cement pastes with organic admixture such as citric acid (Schner et al., 2009). Wang et al. (2021) attributed this increase of ettringite to the higher concentrations of Ca^{2+} and SO_4^{2+} in the pore solution induced by the presence of macromolecular groups.

At 28d, the content of CH in the TA paste is only slightly lower than that of the control one, suggesting that the retarding effect of TA is very limited at late age, as shown in Figs. 8(b) and 9(b). Although hydrations of CNS and CNS+TA pastes were promoted according to calorimetry testing shown in Fig. 6, the CH contents in these two pastes are much lower than the control one because of the pozzolanic reaction between the CH and the CNS. Fig. 9(b) shows that the content of ettringite produced by the CNS+TA paste is higher than that in the CNS paste, suggesting that hydration is more complete in the CNS+TA paste.

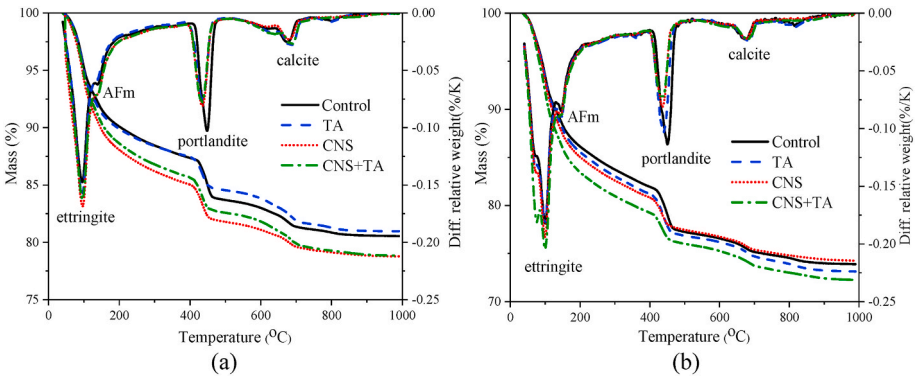

Fig. 8. TGA results of cement pastes at: (a) 2d; (b) 28d.

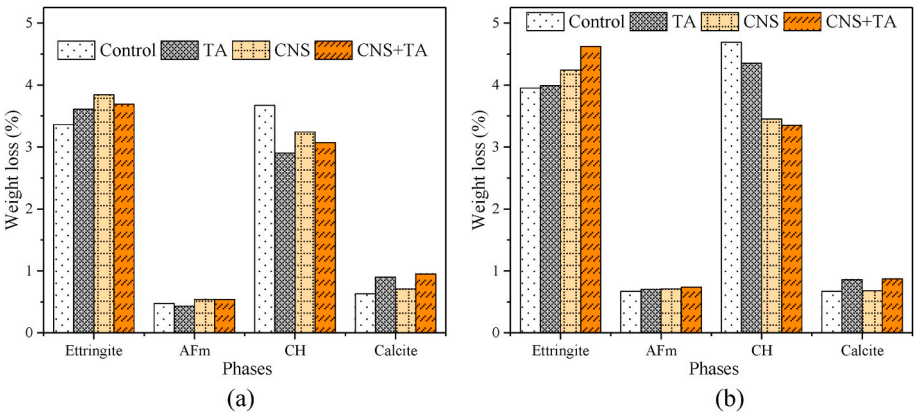

Fig. 9. Weight losses of different minerals at: (a) 2d; (b) 28d.

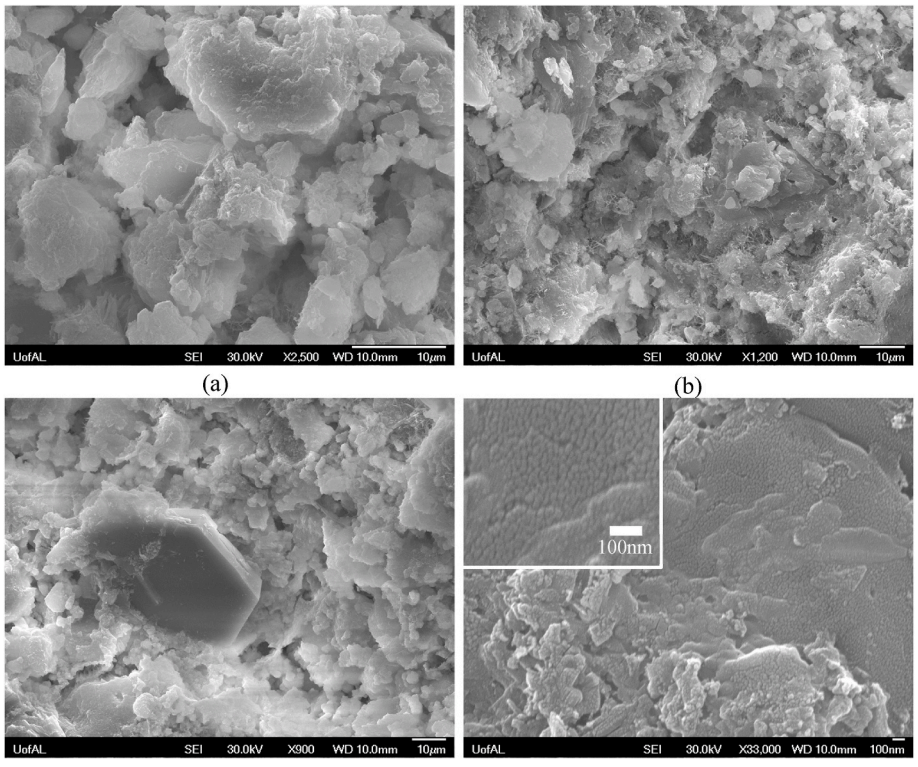

Fig. 10. SEM images of cement pastes at 28d: (a) Control; (b) CNS+TA; (c) CNS; (d) TA.

3.5. Microstructure

Fig. 10 shows the representative microstructures of the cement pastes produced with and without TA dispersed CNS. Comparing Fig. 10 (a) and (b), it can be found that cement paste with the bio-hybrid nanoparticles has a much denser microstructure than the control one. Much more micropores or cracks can be observed on the control specimen shown in Fig. 10(a). Fig. 10(c) shows the SEM image of the paste with the pristine CNS, which is also denser than the control specimen. Many hexagonal CH can be found in this paste, whereas no such CH crystal was observed in the paste produced with the TA dispersed CNS. This difference can be attributed to the more homogenous dispersion of CNS induced by the TA in the cement paste, leading to a more complete pozzolanic reaction at the late age. Fig. 10(b) also shows much more ettringite existing in the CNS+TA specimen, which is in agreement with the result from TGA.

Fig. 10(d) shows the microstructure of the paste with TA. Surprisingly, many nanoparticles with a size of around 20 nm–30 nm were found in this specimen. The result from energy-dispersive X-ray spectroscopy and FTIR showed that these nanoparticles are calcium-TA complex, which was produced at the beginning of the hydration of the cement. Calcium dissolved from cement particles reacted with TA to produce this complex. Since it is insoluble in water, the complex precipitates in the pores of the paste. The presence of TA in the pore solution can prevent further agglomeration of these nanoparticles. This figure clearly indicates that nanoparticles can be in-situ produced in fresh concrete by adding TA.

The MIP tests of cement pastes produced with and without TA dispersed CNS were carried out to further confirm the observation from SEM, and the results are shown in Table 4 and Fig. 11. The total porosity of the cement paste at 28d was reduced from 29.7% to 28.5% by adding the pristine CNS, which is in agreement with existing studies. By using TA dispersed CNS, this porosity was further reduced to 26.5%. The pore size distribution curve presented in Fig. 11(a) shows that adding the pristine CNS refines the pores of the paste. In addition to pore refining, two new features of the pore size distribution can be observed after adding TA dispersed CNS to the paste. First, large pores with size in micrometer in the control sample were eliminated, as indicated by a peak at 2 μm in Fig. 11(a). This can be attributed to the enhanced workability induced by TA dispersion. Second, capillary pores with a size smaller than 50 nm were drastically reduced by adding TA dispersed CNS, as shown in the close-up of the particle size distribution in Fig. 11 (a). These nanopores can also be reduced using the pristine CNS but at a much lower level. This difference in the ability to reduce the nanosize pores in mortar can be attributed to the availability of nanoparticles to fill the pores. Without TA dispersion, CNS can either agglomerate/aggregate to become large particles or react with CH. As a result, much fewer nanoparticles are available to fill the nanopores. While dispersing CNS with TA, biohybrid nanoparticles with a TA coating on the surface are produced. The TA coating can reduce agglomeration/aggregation of nano-silica and retard pozzolanic reaction between CNS and CH. As a result, much more nanoparticles are available to fill those pores with a size smaller than 50 nm, as shown in Fig. 11(a). This reduction in small capillary pores not only increases the strength of concrete but also leads to improvements in drying shrinkage and creep performance of the concrete since these properties of concrete are controlled by nanopores with a size smaller than 30 nm (Jennings et al., 2008).

Table 4
Pore characteristics of cement paste with functionalized CNS as measured by MIP.

Sample	Total Porosity (%)	Average pore diameter (nm)
Control	29.7	33.7
TA	25.8	29.0
CNS	28.5	23.7
CNS+TA	26.5	27.1

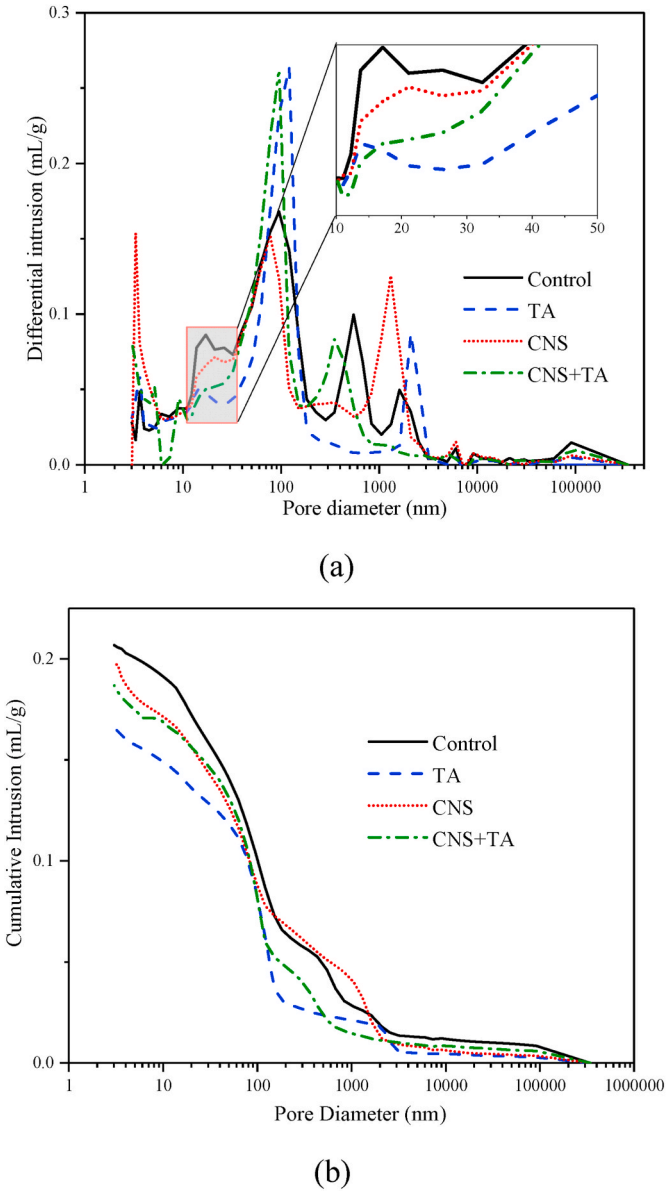

Fig. 11. Pore structure of cement pastes at 28d: (a) pore size distribution; (b) cumulative pore volume.

Table 4 and Fig. 11 also show that the best pore filling is achieved by adding TA. The total porosity is reduced to 25.8%, which is the lowest among all samples. Similarly, the capillary pores smaller than 50 nm of this sample are also minimal among all samples. This is because adding TA into the sample can in-situ produce calcium-TA complex nanoparticles in the mortar to fill the nanopores, as shown in Fig. 10(d), which suggests that the TA can also be used as a new admixture to densify the concrete to achieve better strength and durability. It should be mentioned that TA itself, as a surfactant, can generate bubbles in the mortar during the mixing process. Hence the number of pores around 2 μm was increased in the TA mortar, as shown in Fig. 11.

3.6. Grid of nanoindentation

The TA dispersion of the CNS can not only reduce the porosity by filling the pores but also enable the production of stronger hydration products compared to that of the one without TA, as shown in Fig. 12. In this figure, the area with an elastic modulus higher than 55 GPa is

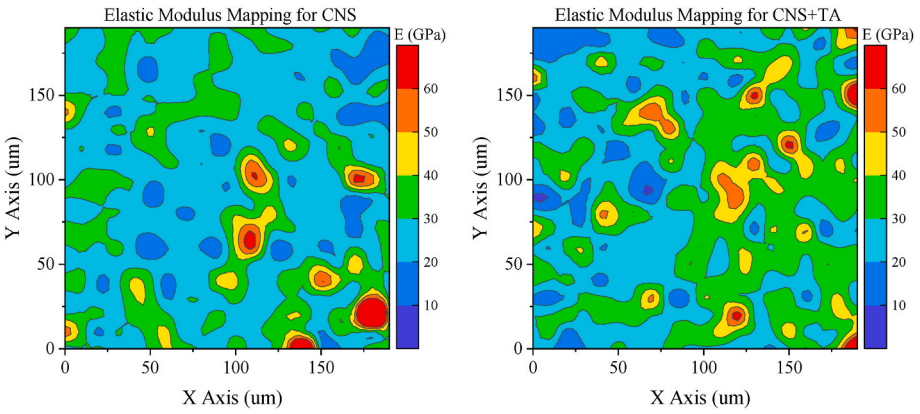

Fig. 12. Elastic modulus maps of the 20*20 nanoindentations of the cement pastes.

mainly composed of non-hydrated clinker (Ulm et al., 2010; Wilson et al., 2017). It can be seen that more high-density C–S–H corresponding to the green area is present on the sample prepared with the TA dispersed CNS, agreeing with the observation obtained by MIP shown in Fig. 11.

Fig. 13 presents deconvolution results to determine the elastic modulus and packing density for CNS and CNS+TA groups. In these figures, π, μ, and σ represent the volume fraction, mean value (in GPa), and standard deviation (in GPa) of each phase, respectively. The average elastic modulus of hydration products produced with CNS dispersed by TA (29.30 GPa) is higher than that prepared with pure CNS (27.92 GPa), which agrees well with the MIP result. As shown in Fig. 11, TA dispersion significantly reduces the pores with a size less than 50 nm, suggesting the hydration products are packed more densely. As a result, the average elastic modulus of the hydration phases measured by the nanoindentation method is higher. Consequently, the micromechanical properties of the produced cement mortars shall be enhanced, which can be confirmed by the compressive strengths of the mortars.

3.7. Compressive strength

Fig. 14 compares the compressive strengths of cement mortars with the mix design detailed in Table 2. As shown in Fig. 14(a), replacing 3% cement with CNS improves the compressive strength of the mortar at 3d, 7d, and 28d by 12%, 6%, and 7%, respectively. This observation agrees with existing studies, which establish that CNS can mainly enhance early-age strength, and its improvement diminishes at late age (Aly et al., 2012; Zeng and Wang, 2016).

After dispersing the CNS with TA, all these strengths were further improved. For example, by using 0.4% TA to disperse CNS, the compressive strengths of the mortar at 3d, 7d, and 28d were improved by 22%, 31%, and 36%, respectively. Increasing the content of TA to 0.6% led to a 44% increase in the compressive strength of the mortar at 28d, as revealed by Fig. 14(a), suggesting that the compressive strength of the mortar at the late age increases with the content of TA used to disperse the CNS. However, the early age strength shows an opposite trend with the content of TA. This can be attributed to the content of free

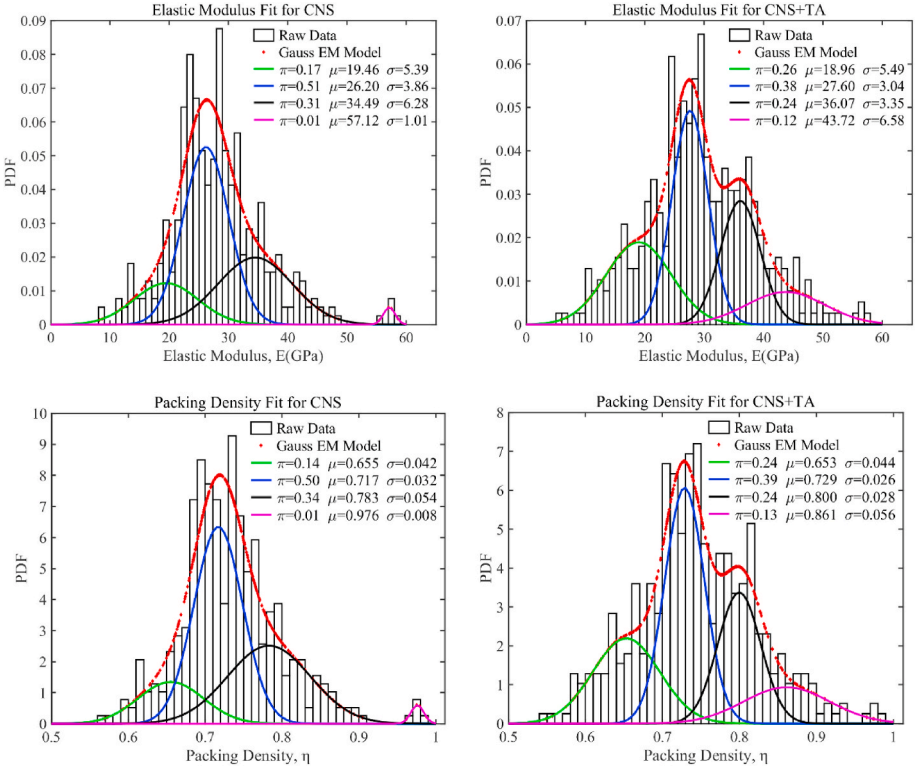

Fig. 13. Deconvolution results of elastic modulus and packing density.

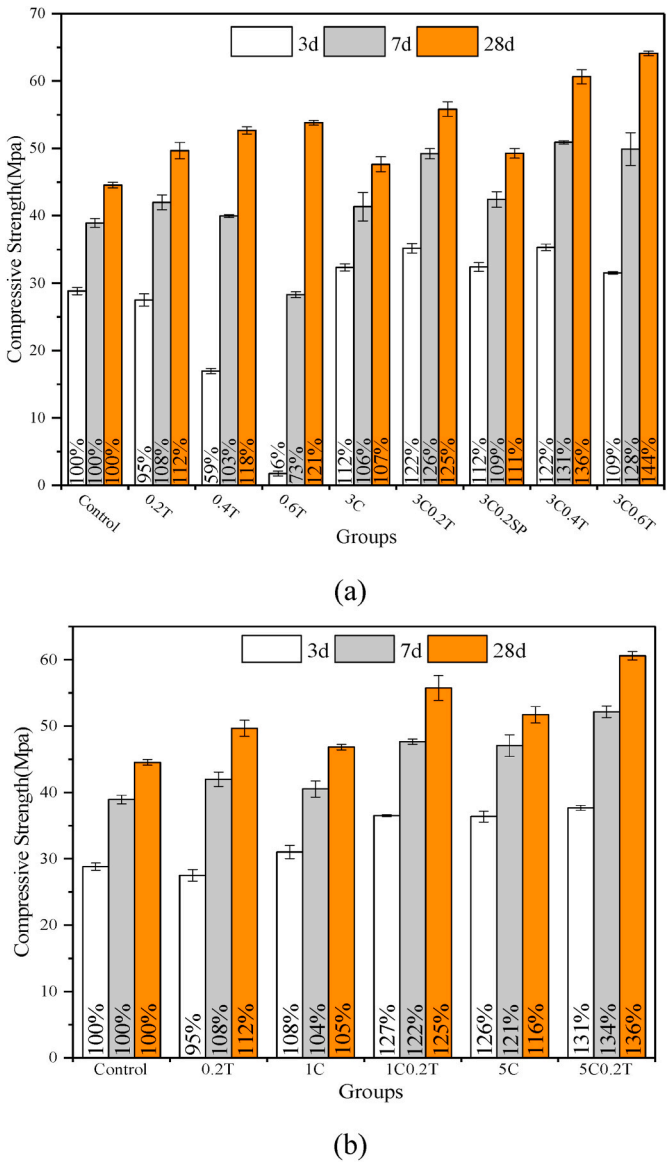

Fig. 14. Compressive strengths of cement mortars prepared with different dosages of CNS: (a) 3%; (b) 1% and 5%.

TA in the mixing water. When TA is used to disperse CNS, some of the TA is adsorbed on the surface of silica nanoparticles to form the biohybrid nanoparticles, and the rest is present as free TA. The free TA in the mixing water can reduce the porosity of the mortar, as revealed by Fig. 11, and retard the hydration of the cement, as illustrated by Fig. 6. As a result, the presence of more free TA in the mixing water leads to higher late-age strength and lower early-age strength of the mortars. This can also be verified by the compressive strengths of the mortars with only free TA in the mixing water. As shown in Fig. 14, adding 0.2%, 0.4%, and 0.6% of free TA to the mortar improved the compressive strengths of the mortars at 28d by 12%, 18%, and 21%, respectively. However, the compressive strength at 3d was reduced by 5%, 41%, and 94%, respectively. The ability of TA to enhance the strength of the concrete at late age provides an extra benefit of using TA as the dispersant for nanosilica. Moreover, the retarding effect of the TA can be offset by the accelerating effect of the nanosilica.

As revealed by the microstructure shown in Fig. 11 and the micro-mechanical properties shown in Figs. 12 and 13, higher compressive strength achieved by using TA dispersed CNS over the pristine CNS is resulted from the more densely packed hydration products induced by the TA dispersion.

Fig. 14(a) also shows the compressive strength of a mortar (3C0.2SP) in which 3%CNS was dispersed by 0.2% superplasticizer. Compared with the control group, the compressive strength of this mortar was 12%, 9%, and 11% higher at 3d, 7d, and 28d, respectively. This improvement is slightly better than that achieved by the pristine CNS but much lower than that reached by using TA to disperse the CNS. The reason for this advantage of using TA over the superplasticizer to disperse the nanosilica is that the free TA in the solution can in-situ produce nanoparticles in the mortar and, therefore, densify the micro-structure of the hydration products, as revealed by Figs. 11–13.

Fig. 14(b) illustrates the effectiveness of the TA as the dispersant for different doses of the CNS. When replacing 1% of cement with the CNS, the compressive strengths of the produced mortar at 3d, 7d, and 28d were slightly improved by 8%, 4%, and 5%, respectively. After dispersing the CNS with 0.2% TA, these compressive strengths were improved by 27%, 22%, and 25%, respectively. When the CNS content was increased to 5%, the compressive strengths of the mortar at 3d, 7d, and 28d were improved by 26%, 21%, and 16%, respectively. This improvement can be augmented by dispersing the CNS with 0.2% TA. As shown in Fig. 14(b), the compressive strengths at these three ages were enhanced by 31%, 34%, and 36%, respectively.

4. Conclusions

This study examines the effectiveness of using tannic acid as a clean dispersant for CNS in cement mortars. Due to its strong adhesion ability, TA can be adsorbed on the surface of silica nanoparticles to form a SiO_2-TA core-shell biohybrid nanoparticles. The TA shell reduces the aggregation/agglomeration of the nanoparticles, leading to better workability of the fresh mortar. Experimental studies suggest that the pozzolanic reaction between the nano-silica and CH in the mortar was retarded by the TA shell, making more nanosilica available to fill the nanopores in the mortar. As a result, a significant reduction of the capillary pores with size smaller than 50 nm is induced in the mortar with TA dispersed CNS. This change of the microstructure leads to a higher elastic modulus of the hydrate products measured by nanoindentation and a much higher compressive strength of the mortar. This study also reveals the great potential of naturally occurring products such as TA as a truly clean dispersant for nanosilica. Compared with petroleum-based dispersants, these natural dispersants enjoy many advantages. They are not only non-toxic but also renewable, low-cost, and widely available, providing a viable solution to decarbonize the chemical admixtures for concretes.

CRediT authorship contribution statement

Xin Qian: Investigation, Writing – original draft, preparation. **Jialai Wang:** Conceptualization, Funding acquisition, Investigation, Writing – review & editing. **Liang Wang:** Investigation. **Yi Fang:** Writing – review & editing, Supervision. **Peiyuan Chen:** Investigation. **Mengxiao Li:** Investigation.

Declaration of competing interest

The authors declare that they have no known competing financial interests or personal relationships that could have appeared to influence the work reported in this paper.

Data availability

Data will be made available on request.

Acknowledgements

The financial support from the U.S. National Science Foundation (CMMI# 1563551 and CMMI# 1761672) and National Natural Science

Foundation of China (51908418) are highly appreciated.

References

Abhilash, P.P., Nayak, D.K., Sangoju, B., Kumar, R., Kumar, V., 2021. Effect of nano-silica in concrete; a review. Construct. Build. Mater. https://doi.org/10.1016/j.conbuildmat.2021.122347.

Abrams, D., 1920. Effect of Tannic Acid on the Strength of Concrete.

Aly, M., Hashmi, M.S.J., Olabi, A.G., Messeiry, M., Abadir, E.F., Hussain, A.I., 2012. Effect of colloidal nano-silica on the mechanical and physical behaviour of waste-glass cement mortar. Mater. Des. 33, 127–135. https://doi.org/10.1016/j.matdes.2011.07.008.

ASTM, 2021a. C39/C39M-21:Standard Test Method for Compressive Strength of Cylindrical Concrete Specimens. West Conshohocken, PA.

ASTM, 2017. C1702-17: Standard Practice for Measurement of Heat of Hydration of Hydraulic Cementitious Materials Using Isothermal Conduction Calorimetry. https://doi.org/10.1520/C1702-17. West Conshohocken, PA.

ASTM, 2015. C1437-15:Standard test method for flow of hydraulic cement mortar. Standard 7–8. https://doi.org/10.1520/C1437-13.2.

ASTM, 2014. C1679-14: Measuring Hydration Kinetics of Hydraulic Cementitious Mixtures Using Isothermal Calorimetry. https://doi.org/10.1520/C1679-14.

ASTM, 2021b. C191−21: Standard Test Methods for Time of Setting of Hydraulic Cement by Vicat Needle. West Conshohocken, PA.

Borges, P.H.R., Costa, J.O., Milestone, N.B., Lynsdale, C.J., Streatfield, R.E., 2010. Carbonation of CH and C-S-H in composite cement pastes containing high amounts of BFS. Cement Concr. Res. 40, 284–292. https://doi.org/10.1016/j.cemconres.2009.10.020.

Chen, C., Yang, H., Yang, X., Ma, Q., 2022. Tannic acid: a crosslinker leading to versatile functional polymeric networks: a review. RSC Adv. https://doi.org/10.1039/d1ra07657d.

Chithra, S., Senthil Kumar, S.R.R., Chinnaraju, K., 2016. The effect of Colloidal Nano-silica on workability, mechanical and durability properties of High Performance Concrete with Copper slag as partial fine aggregate. Construct. Build. Mater. 113, 794–804. https://doi.org/10.1016/j.conbuildmat.2016.03.119.

Collodetti, G., Gleize, P.J.P., Monteiro, P.J.M., 2014. Exploring the potential of siloxane surface modified nano-SiO2to improve the Portland cement pastes hydration properties. Construct. Build. Mater. 54, 99–105. https://doi.org/10.1016/j.conbuildmat.2013.12.028.

Fang, Y., Wang, J., Qian, X., Wang, L., Dong, Y., Qiao, P., 2021. Low-cost, ubiquitous biomolecule as a strength enhancer for cement mortars. Construct. Build. Mater. 311, 125305 https://doi.org/10.1016/j.conbuildmat.2021.125305.

Fei, X., Wei, W., Zhao, F., Zhu, Y., Luo, J., Chen, M., Liu, X., 2017. Efficient toughening of epoxy-anhydride thermosets with a biobased tannic acid derivative. ACS Sustain. Chem. Eng. 5, 596–603. https://doi.org/10.1021/acssuschemeng.6b01967.

Fernández, J.M., Duran, A., Navarro-Blasco, I., Lanas, J., Sirera, R., Alvarez, J.I., 2013. Influence of nanosilica and a polycarboxylate ether superplasticizer on the performance of lime mortars. Cement Concr. Res. 43, 12–24. https://doi.org/10.1016/j.cemconres.2012.10.007.

Gao, R.J., Yao, Y., Wu, H., Wang, L., 2017. Effect of amphoteric dispersant on the dispersion properties of nano-SiO2particles. J. Appl. Polym. Sci. 134, 1–8. https://doi.org/10.1002/app.45075.

Gu, Y., Ran, Q., Shu, X., Yu, C., Chang, H., Liu, J., 2016. Synthesis of nanoSiO2@PCE core-shell nanoparticles and its effect on cement hydration at early age. Construct. Build. Mater. 114, 673–680. https://doi.org/10.1016/j.conbuildmat.2016.03.093.

Hagerman, A.E., Riedl, K.M., Jones, G.A., Sovik, K.N., Ritchard, N.T., Hartzfeld, P.W., Riechel, T.L., 1998. High molecular weight plant polyphenolics (Tannins) as biological antioxidants. J. Agric. Food Chem. 46, 1887–1892. https://doi.org/10.1021/jf970975b.

Hashem, F.S., Amin, M.S., El-Gamal, S.M.A., 2013. Improvement of acid resistance of Portland cement pastes using rice husk ash and cement kiln dust as additives. J. Therm. Anal. Calorim. 111, 1391–1398. https://doi.org/10.1007/s10973-012-2458-4.

Jennings, H.M., Bullard, J.W., Thomas, J.J., Andrade, J.E., Chen, J.J., Scherer, G.W., 2008. Characterization and modeling of pores and surfaces in cement paste. J. Adv. Concr. Technol. 6, 5–29. https://doi.org/10.3151/jact.6.5.

Ju, S.W., Prajatelistia, E., Jun, S.H., Hwang, D.S., Ahn, J.S., Sanandiya, N.D., 2017. Aesthetically improved and efficient tannin-metal chelates for the treatment of dentinal hypersensitivity. RSC Adv. 7, 87–94. https://doi.org/10.1039/c6ra24745h.

Kong, D., Pan, H., Wang, L., Corr, D.J., Yang, Y., Shah, S.P., Sheng, J., 2019. Effect and mechanism of colloidal silica sol on properties and microstructure of the hardened cement-based materials as compared to nano-silica powder with agglomerates in micron-scale. Cem. Concr. Compos. 98, 137–149. https://doi.org/10.1016/j.cemconcomp.2019.02.015.

Kong, D., Su, Y., Du, X., Yang, Y., Wei, S., Shah, S.P., 2013. Influence of nano-silica agglomeration on fresh properties of cement pastes. Construct. Build. Mater. 43, 557–562. https://doi.org/10.1016/j.conbuildmat.2013.02.066.

Korayem, A.H., Tourani, N., Zakertabrizi, M., Sabziparvar, A.M., Duan, W.H., 2017. A review of dispersion of nanoparticles in cementitious matrices : nanoparticle geometry perspective. Construct. Build. Mater. 153, 346–357. https://doi.org/10.1016/j.conbuildmat.2017.06.164.

Kusmierek, E., Chrzescijanska, E., 2015. Tannic acid as corrosion inhibitor for metals and alloys. Mater. Corros. 66, 169–174. https://doi.org/10.1002/maco.201307277.

Li, G., Yue, J., Guo, C., Ji, Y., 2018. Influences of modified nanoparticles on hydrophobicity of concrete with organic film coating. Construct. Build. Mater. 169, 1–7. https://doi.org/10.1016/j.conbuildmat.2018.02.191.

Liu, J., Chen, H., Xu, Z., Zheng, S., Xue, M., 2015. Adsorption of tannic acid from aqueous solution by aminopropyl functionalized SBA-15. Desalination Water Treat. 56, 475–484. https://doi.org/10.1080/19443994.2014.940394.

Lu, Z., Kong, X., Zhang, C., Xing, F., Cai, Y., Jiang, L., Zhang, Y., Dong, B., 2017. Effect of surface modification of colloidal particles in polymer latexes on cement hydration. Construct. Build. Mater. 155, 1147–1157. https://doi.org/10.1016/j.conbuildmat.2017.08.114.

Mukharjee, B.B., Barai, S.V., 2020. Influence of incorporation of colloidal nano-silica on behaviour of concrete. Iran. J. Sci. Technol. - Trans. Civ. Eng. 44, 657–668. https://doi.org/10.1007/s40996-020-00382-0.

Oliver, W.C., Pharr, G.M., 1992. An improved technique for determining hardness and elastic modulus using load and displacement sensing indentation experiments. J. Mater. Res. 7 https://doi.org/10.1557/jmr.1992.1564.

Park, H., Jeong, Y., Jeong, J.H., Oh, J.E., 2016. Strength development and hydration behavior of self-activation of commercial ground granulated blast-furnace slag mixed with purified water. Materials 9, 11. https://doi.org/10.3390/ma9030185.

Pedrosa, H.C., Reales, O.M., Reis, V.D., Paiva, M., das, D., Fairbairn, E.M.R., 2020. Hydration of Portland cement accelerated by C-S-H seeds at different temperatures. Cement Concr. Res. 129, 105978 https://doi.org/10.1016/j.cemconres.2020.105978.

Pellenq, R.J.M., Kushima, A., Shahsavari, R., Van Vliet, K.J., Buehler, M.J., Yip, S., Ulm, F.J., 2009. A realistic molecular model of cement hydrates. Proc. Natl. Acad. Sci. U. S. A. 106, 16102–16107. https://doi.org/10.1073/pnas.0902180106.

Schieber, A., Stintzing, F., Carle, R., 2001. By-products of plant food processing as a source of functional compounds — recent developments. Trends Food Sci. Technol. 12, 401–413. https://doi.org/10.1016/S0924-2244(02)00012-2.

Schner, M., Lothenbach, G.B., Figi, R., Kretzschmar, R., 2009. Influence of citric acid on the hydration of Portland cement. Cement Concr. Res. 39 (4), 275–282.

Shnawa, H.A., Khalaf, M.N., Jahani, Y., Taobi, A.A.H., 2015. Efficient thermal stabilization of polyvinyl chloride with tannin-Ca complex as bio-based thermal stabilizer. Mater. Sci. Appl. 360–372. https://doi.org/10.4236/msa.2015.65042, 06.

Ulm, F.J., Vandamme, M., Jennings, H.M., Vanzo, J., Bentivegna, M., Krakowiak, K.J., Constantinides, G., Bobko, C.P., Van Vliet, K.J., 2010. Does microstructure matter for statistical nanoindentation techniques? Cem. Concr. Compos. 32, 92–99. https://doi.org/10.1016/j.cemconcomp.2009.08.007.

Vandamme, M., 2008. The nanogranular origin of concrete creep : a nanoindentation investigation of microstructure and fundamental properties of calcium-silicate-hydrates. Environ. Eng. 366.

Vandamme, M., Ulm, F., 2013. Nanoindentation investigation of creep properties of calcium silicate hydrates. Cement Concr. Res. 52, 38–52. https://doi.org/10.1016/j.cemconres.2013.05.006.

Wang, L., Ju, S., Wang, L., Wang, F., Sui, S., Yang, Z., Liu, Z., Chu, H., Jiang, J., 2021. Effect of citric acid-modified chitosan on the hydration and microstructure of Portland cement paste. J. Sustain. Cement-Based Mater. 1–14.

Wilson, W., Rivera-Torres, J.M., Sorelli, L., Durán-Herrera, A., Tagnit-Hamou, A., 2017. The micromechanical signature of high-volume natural pozzolan concrete by combined statistical nanoindentation and SEM-EDS analyses. Cement Concr. Res. 91, 1–12. https://doi.org/10.1016/j.cemconres.2016.10.004.

Zeng, S., Wang, J., 2016. Characterization of mechanical and electric properties of geopolymers synthesized using four locally available fly ashes. Construct. Build. Mater. 121, 386–399. https://doi.org/10.1016/j.conbuildmat.2016.06.011.

Zhuravlev, L.T., 2000. The surface chemistry of amorphous silica. Zhuravlev model. Colloids Surf. A Physicochem. Eng. Asp. 173, 1–38. https://doi.org/10.1016/S0927-7757(00)00556-2.